ORIGINAL PAPER

Heating-Dominated Fracturing of Granite by Open-Ended Microwave: Insights from Acoustic Emission Measurement

Yanlong Zheng[1] · Zhongjun Ma[1] · Qiuming Gong[2] · Penghai Zhang[3] · Xiaobao Zhao[4] · Jianchun Li[1]

Abstract

Microwave fracturing of hard rocks holds great promise in the civil, mining and tunnelling industries. The role of heating and cooling in the fracturing of rocks and when and where cracks initiate from and propagate to remain unclear and need to be addressed for future field applications of the technology. This study treated an alkali feldspar granite using a 6 kW industrial microwave source and a customised open-ended dielectric-loaded converging waveguide antenna. The real-time acoustic emission (AE) characteristics in the microwave heating and natural cooling phases were recorded and investigated. The surface temperature and P-wave velocity reduction of the specimens were also measured to quantify the thermal damage. The fracturing of granite is found to be tensile failure and is heating-dominated. Although a considerable amount of AE hits and events was detected in the cooling phase, they were of low energy, and therefore, the role of cooling in rock fracturing by open-ended microwave can be neglected. Fractures initiated from the exterior of the antenna and propagated towards the edges and the interior of the specimens. The cracks obtained from the AE localisation were in good agreement with those observed. With the increase of power level, the time for crack initiation was shortened, confirming the high-power effect.

Highlights

- Acoustic emission activities were measured in the microwave heating and cooling phases on granite blocks.
- Microwave fracturing of the granite is found to be heating-dominated.
- The microwave-induced rock fracturing is primarily tensile failure.
- The test results confirm the high-power effect in microwave fracturing of rocks.

✉ Yanlong Zheng
yanlong.zheng@seu.edu.cn

✉ Jianchun Li
jcli@seu.edu.cn

1 Institute of Underground Space, School of Civil Engineering, Southeast University, Nanjing 211189, China

2 Key Laboratory of Urban Security and Disaster Engineering of Ministry of Education, Beijing University of Technology, Beijing 100124, China

3 Key Laboratory of Ministry of Education on Safe Mining of Deep Metal Mines, Northeastern University, Shenyang 110819, China

4 School of Earth Sciences and Engineering, Nanjing University, Nanjing 210093, China

1 Introduction

The use of microwave treatment to weaken hard and abrasive rocks prior to mechanical breakage has re-emerged as a hot research topic in the past decade (Wei et al. 2019; Zheng and He 2021; Xu et al. 2021). After microwave treatment, the uniaxial compressive strength (UCS) (Hassani et al. 2016; Yang et al. 2022; Kahraman et al. 2020), Brazilian tensile strength (Hassani et al. 2016; Kahraman et al. 2020), point load strength (Whittles et al. 2003; Kingman et al. 2004), elastic modulus (Zheng et al. 2020), ultrasonic wave velocity (Zheng et al. 2020; Lu et al. 2019), dynamic UCS (Wang et al. 2020), dynamic fracture toughness (Li et al. 2020b; Bai et al. 2021) and dynamic tensile strength

(Li et al. 2020a) can be substantially reduced. Microwave treatment also fractures rocks to assist the mechanical rock breakage (Ma et al. 2021b; Hartlieb et al. 2017). The technology has great potential in increasing the rock breaking efficiency of mechanical excavators (Hartlieb et al. 2017; Kahraman et al. 2022), reducing the environmental impacts (vibration and noise), and reducing the energy consumption (Ma et al. 2021b).

Microwave fractures hard rocks by the following two mechanisms: (1) It selectively heats and vaporises water in closed pores and the specimens either spall or break explosively (Zhao et al. 2020). The former happens in porous extrusive rocks, such as basalt, while the latter happens in sedimentary rocks, such as sandstone and slate (Chen et al. 2015). This mechanism also applies to selectively heating and melting of high-microwave absorbing minerals in the gangue matrix, for instance, pyrite inclusion in the rock matrix (Zheng et al. 2020). (2) It could generate high enough thermal stresses and mismatches to break rocks. The local fracturing takes place in the high temperature zone and is a result from the difference in thermal expansion coefficients of minerals and the anisotropy of thermal expansion within single minerals (Hartlieb et al. 2017; Ma et al. 2021b). The global fracturing results from the thermal gradients by rapid microwave heating (Hartlieb et al. 2017; Ma et al. 2021b). The temperature gradient can reach up to 40 ℃/mm when using a 6 kW microwave source and a dielectric-loaded converging waveguide antenna (DLCWA) (Ma et al. 2021a).

To simulate the field scenario of microwave fracturing of rocks at a tunnel face or a rock bench, an industrial microwave source and an open-ended antenna should be used (Ma et al. 2021b; Lu et al. 2019; Feng et al. 2021). Those tests usually involve large size specimens. Since microwave irradiation can be detrimental to staff and instruments, such as thermal and optical cameras, it is very hard to perform real-time measurement of the temperature and to quantify the damage (Council 1994). This is one of the main reasons why measurements such as temperature, ultrasonic wave velocity and cracking are performed when microwave heating stops, even when the specimen completely cools down. This methodology makes it technically challenging to instantaneously monitor and localise the fracturing activities and the damage.

The acoustic emission (AE) method as a non-destructive evaluation technique has been extensively used in the research of progressive micro-cracking of rock specimens under different loading conditions and thermal treatment (Yin et al. 2014; Du et al. 2020; Grosse and Ohtsu 2008; Guo et al. 2021; Li et al. 2021; Lyu et al. 2021; Wu et al. 2021; Yang et al. 2020). AE detectors capture the AE signals generated by the formation of local damage in the rocks, allowing researchers to determine how much microcracking and damage is induced and to localize the cracks

(Zhang and Deng 2020; Zhang et al. 2020). The evolution of microcracks and the fracture modes can be analysed based on the b value and the ratio of the rise angle and the average frequency (RA/AF) (Ge and Sun 2018; Peng et al. 2018; Zhang and Deng 2020). However, in the literature, the AE technique was only used to study the behaviours of rocks after microwave treatment under uniaxial loading (Ge and Sun 2021; Lu et al. 2021). No attempts except Feng et al. (2021) have been made to investigate the real-time evolution of rock fracturing in the microwave heating and natural cooling phases. According to Browning et al. (2016), the cooling phase in conventional thermal treatment may induce more fracturing to the specimens than the heating phase. Since microwave heating induces thermal shock, the role of the natural cooling phase in the fracturing of rocks is, therefore, subjected to further exploration.

The objective of this paper is to investigate the real-time fracturing of granite in the microwave heating and natural cooling phases using the AE technique. The microwave heating was performed using a 6 kW industrial microwave source and a customized open-ended DLCWA. The surface temperature and P-wave velocity reduction of the specimens were measured to characterize the thermal damage. The AE characteristics in the microwave heating and natural cooling phases were then examined to reveal the initiation and propagation and failure mode of the cracks as well as the role heating and cooling play in microwave fracturing of the granite.

2 Materials and Methodologies

2.1 Rock Specimens

The tested granite was taken from a quarry in Hubei province, China. Figure 1 shows the images of the granite under normal and cross-polarised light. The petrographic analysis indicates that it is composed of 50% alkali feldspar, 8% plagioclase, 36% quartz, 5% biotite, and 1% muscovite. The alkali feldspar granite is a medium-grained rock with a mean grain size of approx. 2 mm. It has a density of 2610 kg/m^3, a UCS of 75 MPa, and a P-wave velocity of 4800 m/s. The strength of the granite is relatively low due to slight weathering. Due to the low values in strength, P-wave velocity and dielectric loss factor, the granite has a relatively low microwave fracturability index (MFI) and is relatively difficult to be fractured by microwave (Zheng et al. 2021). Therefore, either a high power density or a long heating duration is needed to fracture it. In the tests, cubic specimens with an edge length of 250 mm were prepared.
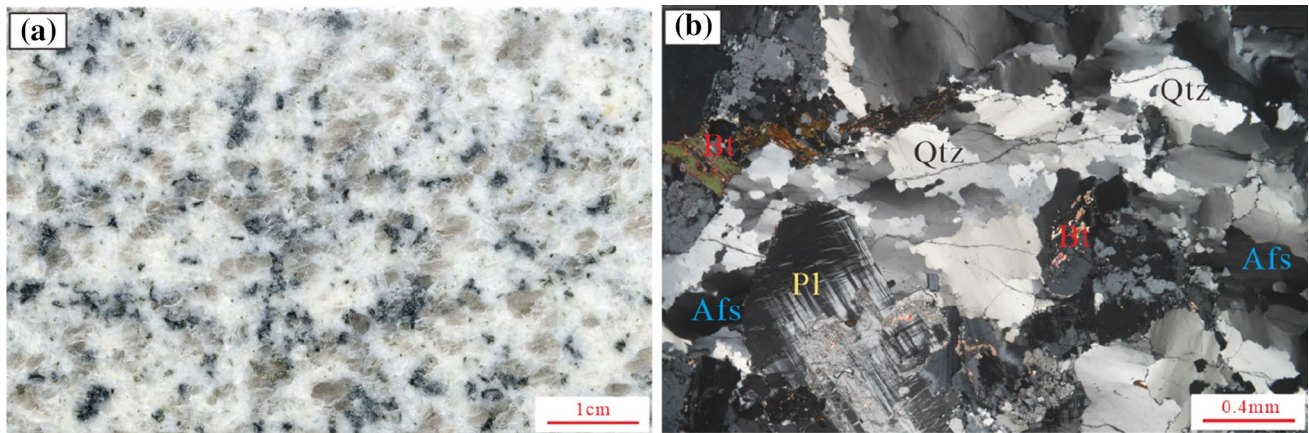
Fig. 1 Optical images of the granite under **a** normal light and **b** cross-polarised light. *Bt* biotite, *Afs* Alkali feldspar, *Pl* plagioclase, *Qtz* quartz

2.2 Experimental Setup and Instrumentation

The microwave treatment of the granite specimens using an open-ended DLCWA is illustrated in Fig. 2. The setup consists of a microwave isolating metallic container, a 6 kW SAIREM industrial microwave source, a DLCWA with an aperture size of 40 mm × 30 mm and an AE measurement system. The components and functions of the microwave source (Model: GMP G4) are referred to Zheng et al. (2017) and Ma et al. (2021b). The DLCWA was customized to focus microwave power to a high enough intensity to fracture the low-MFI rocks (Ma et al. 2021a). At 6 kW, the maximum power intensity on the rock surface is approx. 1200 W/cm^2. In this study, the end of the antenna was in contact with the surface centre of the rock specimens which were placed on a lifting platform with position adjusting capacities. This setup could simulate the field scenario of microwave fracturing of rocks to the greatest possible extent.

An 8-channel AE measurement system, PCI-8 from Physical Acoustics Corporation, was employed for real-time monitoring of the crack initiation and propagation as well as rock damage during the microwave heating and cooling process. AE parameters including waveform, hit, count, energy, and event were recorded. The layout of the AE sensors is shown in Figs. 2 and 3. Six sets of R6α sensors with a diameter of 19 mm and an operation range from 35 to 100 kHz were attached on the front and back surface of the rock specimens with two rubber bands. The front sensors were in an inverted triangle, the back sensors in a regular triangle, and the distance between each sensor and the boundary is 40 mm. The sensors, the connecting wire and the contact area were wrapped by aluminium foil to protect them from microwave damage (Fig. 3). Considering the background noise, the AE trigger level was set to 40 dB. The sampling rate was 3 million samples per second (MSPS). The time parameters for the AE signals definition, namely,

peak definition time (PDT), hit definition time (HDT), and hit lockout time (HLT), were set as 50, 100, and 200 μs, respectively.

An infrared temperature imager (Model: FLIR T420), with a range is 20–650 °C and an accuracy is ± 2 °C or ± 2% (whichever is greater) was used to measure the surface temperature of specimens. The P-wave velocity at the radiation centre across the total thickness was measured using an ultrasonic velocity tester (Model: Sinorock RSM-SY6). The cracks were recorded with the help of a portable microscope.

2.3 Experimental Procedure

The experiments strictly followed the procedure below:

(1) Measure the initial P-wave velocity and initial surface temperature of a specimen;
(2) Lay the rock specimen on the lifting platform, attach the AE sensors on the front and back surfaces of the specimen and then adjust the AE system;
(3) Microwave heat the specimen at the designed power level (3–6 kW) for a specific duration (1–4 min) and monitor the real-time AE signals;
(4) Measure the surface temperature distribution of the specimen immediately after heating stops, record the crack information, and continuously monitor the AE signals for a 10-min natural cooling phase;
(5) Measure the P-wave velocity of the specimen when it cools down;
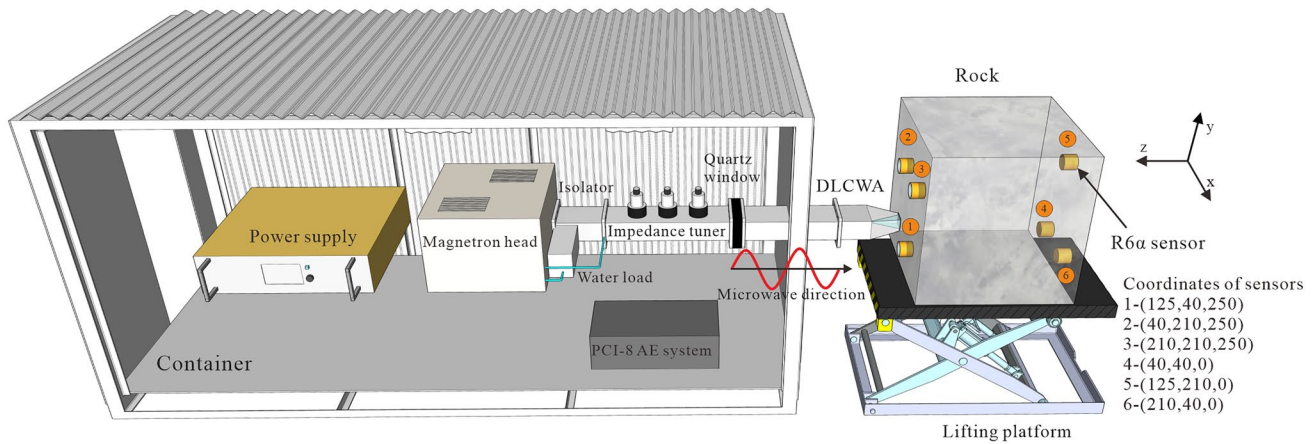(6) Analyse the AE hit, energy, event characteristics in the heating and cooling phases.

Fig. 2 Setup of microwave fracturing of rock blocks and the acoustic emission measurement (Not to scale)

3 Results and Analysis

3.1 Microwave Heating

Figure 4 shows the maximum temperature and ultrasonic wave velocity of the specimens as a function of the heating time and microwave power. It is obvious that there is a highly linear relationship, indicating that the granite is dielectrically stable and there is no thermal run-away. The results confirm the high-power effect of microwave heating which means that for the same energy output a combination of a high microwave power and a short heating duration yields a better heating and damaging effect. For instance, for an energy output of 720 kJ, the maximum temperature at 6 kW for 2 min is 373 °C, substantially higher than that

at 4 kW for 3 min (321 °C). This is also evidenced by the P-wave velocity measurement at the centre, where the former yields a 6.1% reduction, while the reduction for the latter is 4.8%.

3.2 Microwave Fracturing

Fracturing of the granite specimens after microwave treatment is shown in Fig. 5. When the heating duration is short or the power level is low, the microwave is not able to induce visible macrocracks on the granite specimens which have a low MFI. However, as either heating duration or power level increases, more cracks with larger widths on the front treated face and the sides of the specimens were observed. Table 1 summarises the crack info on the specimens after microwave treatment. It clearly
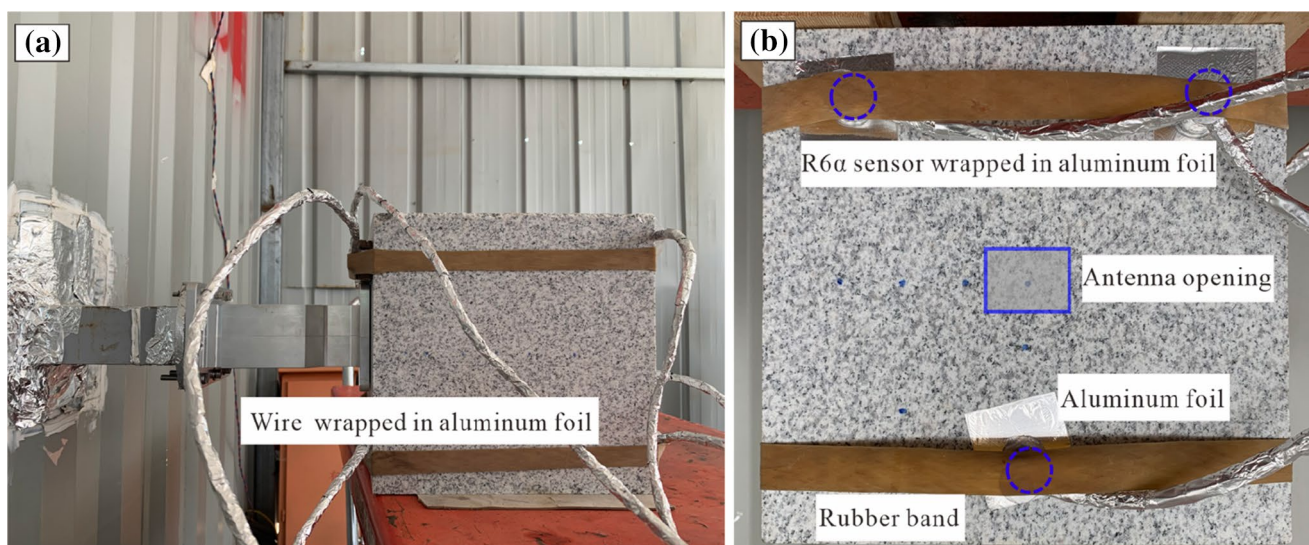

Fig. 3 Layout and protection of the AE sensors and wires. **a** Side view, **b** Front view
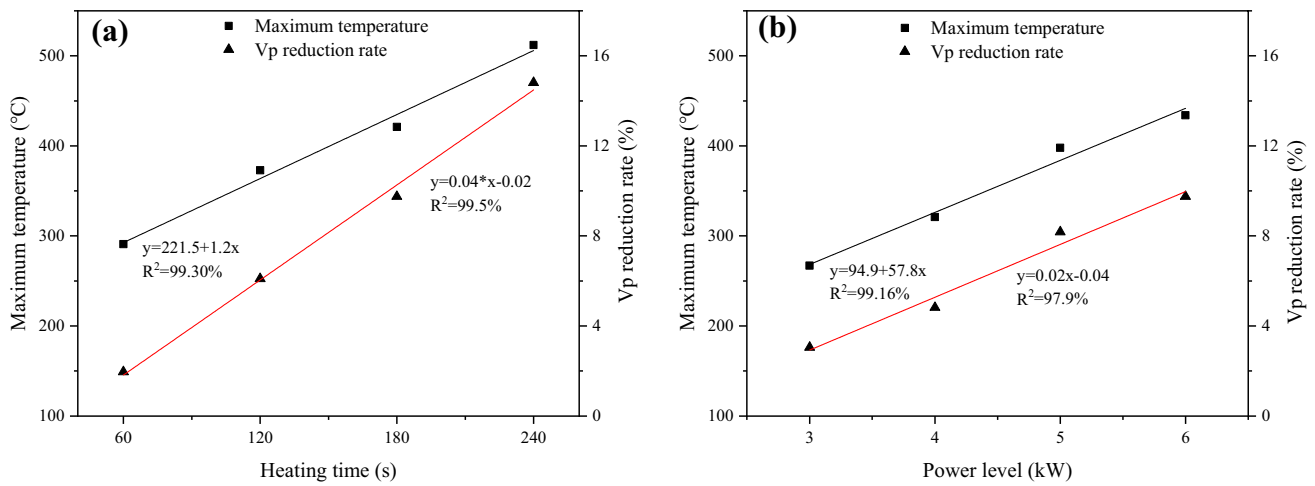
Fig. 4 Maximum temperature and P-wave velocity reduction as a function of **a** heating time at a power of 6 kW and **b** power level for a heating duration of 3 min
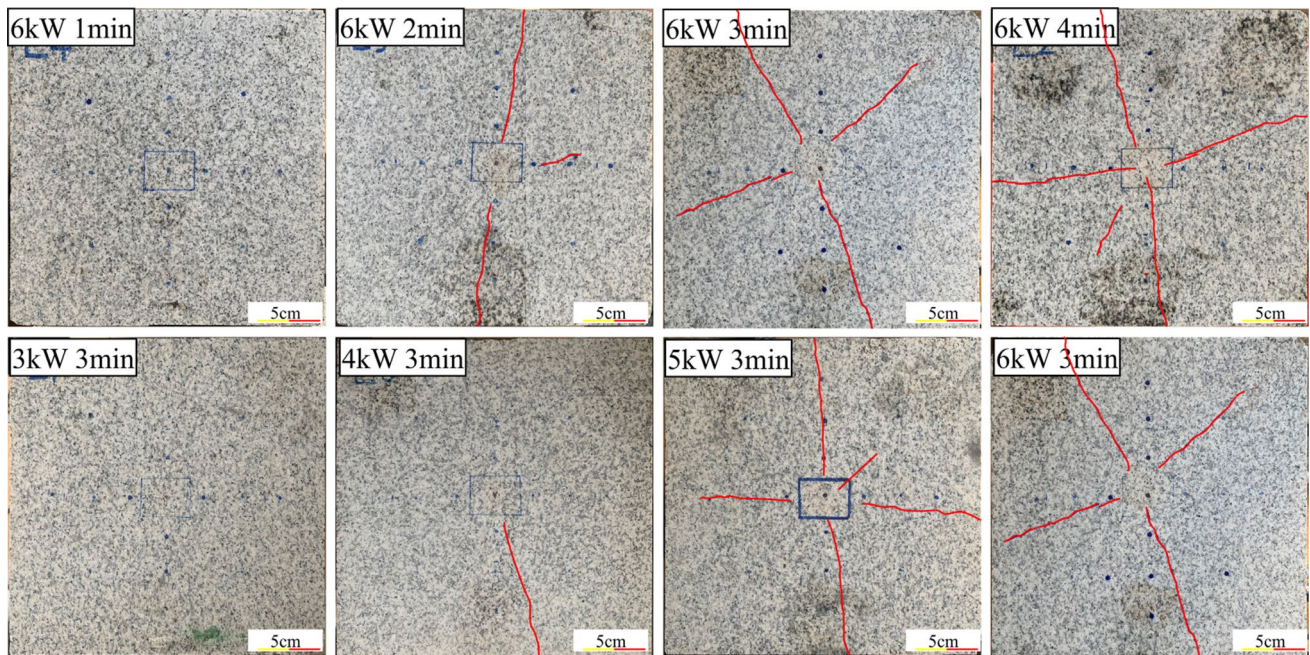

Fig. 5 Microwave fracturing of granite specimens. Top row: at 6 kW for 1–4 min; bottom row: at 3–6 kW for 3 min

demonstrates the performance of the DLCWA in fracturing the low-MFI rock. Table 1 also further confirms the high-power effect, i.e., heating at 6 kW for 2-min induces more and wider cracks on the specimen than at 4 kW for 3 min. This might be attributed to the higher heating rate and higher thermal gradient and stresses. Cracks were in a radial pattern centred on the antenna aperture. The cracks initiate from the exterior of the antenna aperture and propagate towards the edges. The evolution of cracks will be discussed in a later section.

3.3 AE Energy and AE Hits

AE energy is directly associated with the intensity of the AE activities and a jump in the accumulated AE energy is considered to be related to macrocracking (Keshavarz et al. 2010; Kong et al. 2016; Ren et al. 2021; Aker et al. 2014). Figure 6 shows the instantaneous and accumulated AE energy and hits of the specimens treated under different microwave conditions. The AE activities in the heating phase plus a 10-min cooling

Table 1 Summary of the fracture information on the granite specimens after microwave treatment

Power (kW)	Time (min)	Max. temperature (°C)	Total front crack number	Total front crack length (cm)	Total side crack number	Total side crack length (cm)	Max. crack width (mm)
6	1	291	0	0	0	0	0
6	2	373	3	23.8	2	20.8	10.6
6	3	434	4	44.1	2	19.6	11.7
6	4	512	5	51	4	36.7	14.2
5	3	398	4	43.4	2	24	13.5
4	3	321	1	11	1	5.2	5.2
3	3	267	0	0	0	0	0

phase were recorded. However, only the data for the first 5 min is presented in Fig. 6 as the AE hits in the cooling phase were of very low energy and only local microcracks can possibly be generated. At the power of 6 kW, although there were noticeable AE energy and hits in the first minute and in the cooling phase, they were nonetheless negligible (Fig. 6a). Therefore, no cracks were observed on the specimen. With the increase of the heating time, the specimens were fractured at about 100 s. At 6 kW, the AE energy intensity when the specimens began to crack is close (4.5 to 7×10^5 eu). Each AE energy peak corresponds to a macrocracking, which is in good agreement with observations in Fig. 5. After the peak and macrocracking, there were a silent period before the next cracking. It is also obvious in Fig. 6d, e–g that the peak of AE energy and accumulated AE energy increase dramatically as the microwave power increases when the heating time is 3 min.

A quantitative comparison of the AE characteristics during the microwave heating and cooling phases is listed in Table 2. The results show that the AE energy and AE counts during the microwave heating phase are much higher than those in the cooling phase, suggesting that the microwave fracturing of the granite is heating-dominated. This is dramatically different from observations in the conventional heating and cooling phases as conducted by Browning et al. (2016). By contrast, the AE hits and AE events in the microwave heating and natural cooling phases are of the same magnitude. However, the hits and events in the cooling phase are of much lower energy, which can be explained by the fact that in the cooling phase the AE activities come from closure, friction and collision of the cracks. The high-power effect is also validated by the AE energy, i.e., the accumulated AE energy at the end of microwave heating at 6 kW for 2 min is 2.5×10^6 eu, which is significantly higher than that at 4 kW for 3 min, which is 6.8×10^4 eu.

4 Discussion

4.1 Variation of b Value During the Heating and Cooling

The *b* value, a parameter defined as the log-linear slope of the frequency–magnitude distribution, is proposed in the Gutenberg and Richter relationship (Gutenberg and Richter 1950) and is considered as an effective index for evaluating the fracturing process. The *b* value represents the ratio of the micro-crack frequency and the macro-crack frequency during the fracturing process and it has been widely used to analyse the micro-cracking process in rock mechanics (Ma et al. 2018). A low b value means that a large amount of micro-cracks is developed at this stage (Peng et al. 2018).

In this study, the b-value is calculated by maximum likelihood estimation using the following equation (Nava et al. 2016):

$$b = \frac{20 \lg e}{\overline{A} - A_{\min}} \tag{1}$$

in which e is the base of the natural logarithms (approx. 2.718), $\overline{A}$ is the average AE amplitude measured in dB, $A_{\min}$ is the minimum AE amplitude measured in dB. The window size is set as 2000, and the sliding distance is set as 2000.

Figure 7a shows the relationship between the b value and time for specimens microwaved at 6 kW for 1–4 min. The results show that the b value decreases as the microwave heating time increases. When the heating time was about 100 s, the b value drops dramatically from around 2 to about 0.5, reflecting the generation of large amounts of microcracks and possibly macrocracks. After the

Fig. 6 Instantaneous and accumulated AE energy and hits energy during the microwave heating and cooling phases. **a** 6 kW, 1 min, **b** 6 kW, 2 min, **c** 6 kW, 3 min, **d** 6 kW, 4 min, **e** 5 kW, 3 min, **f** 4 kW, 3 min, **g** 3 kW, 3 min
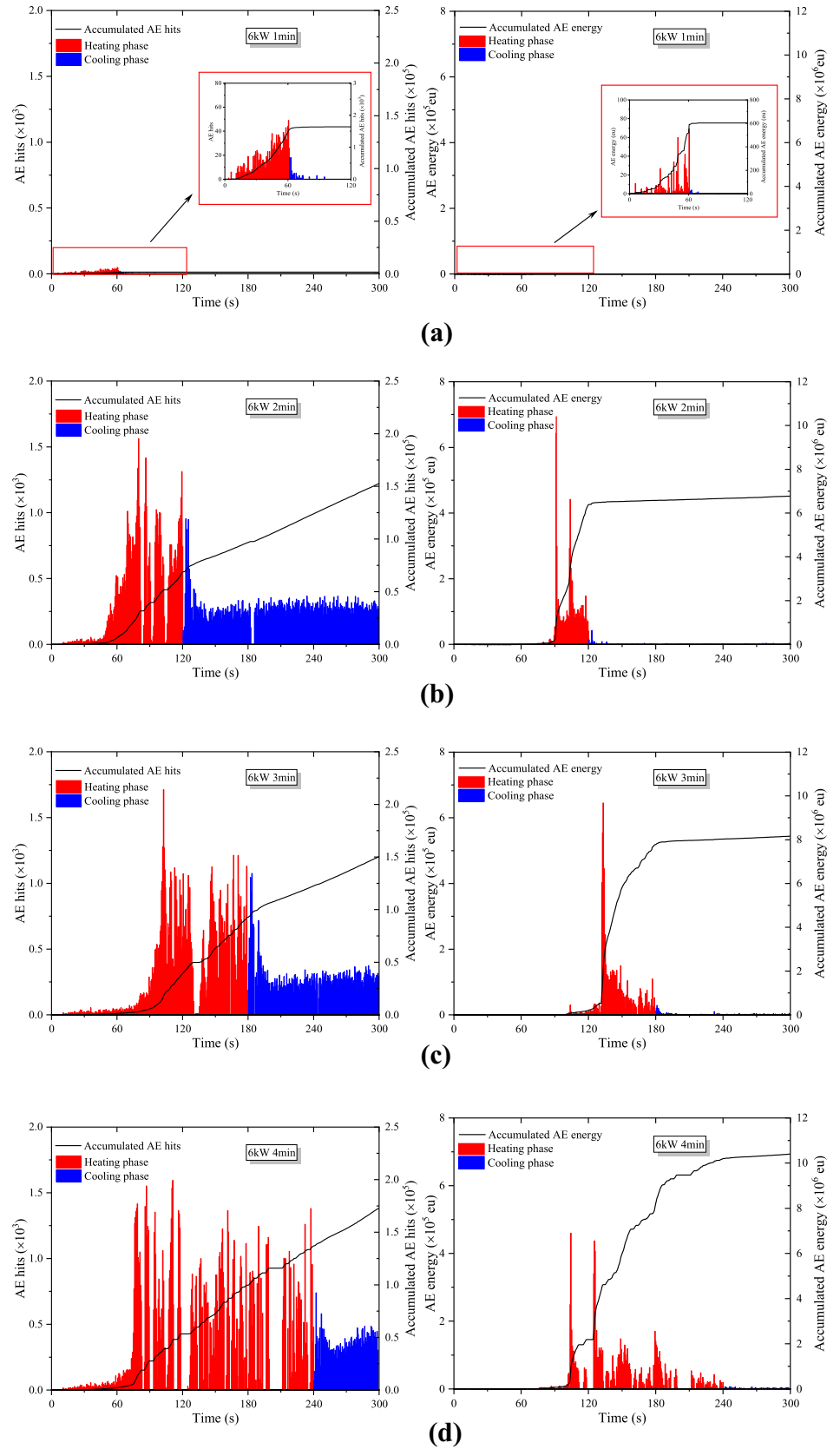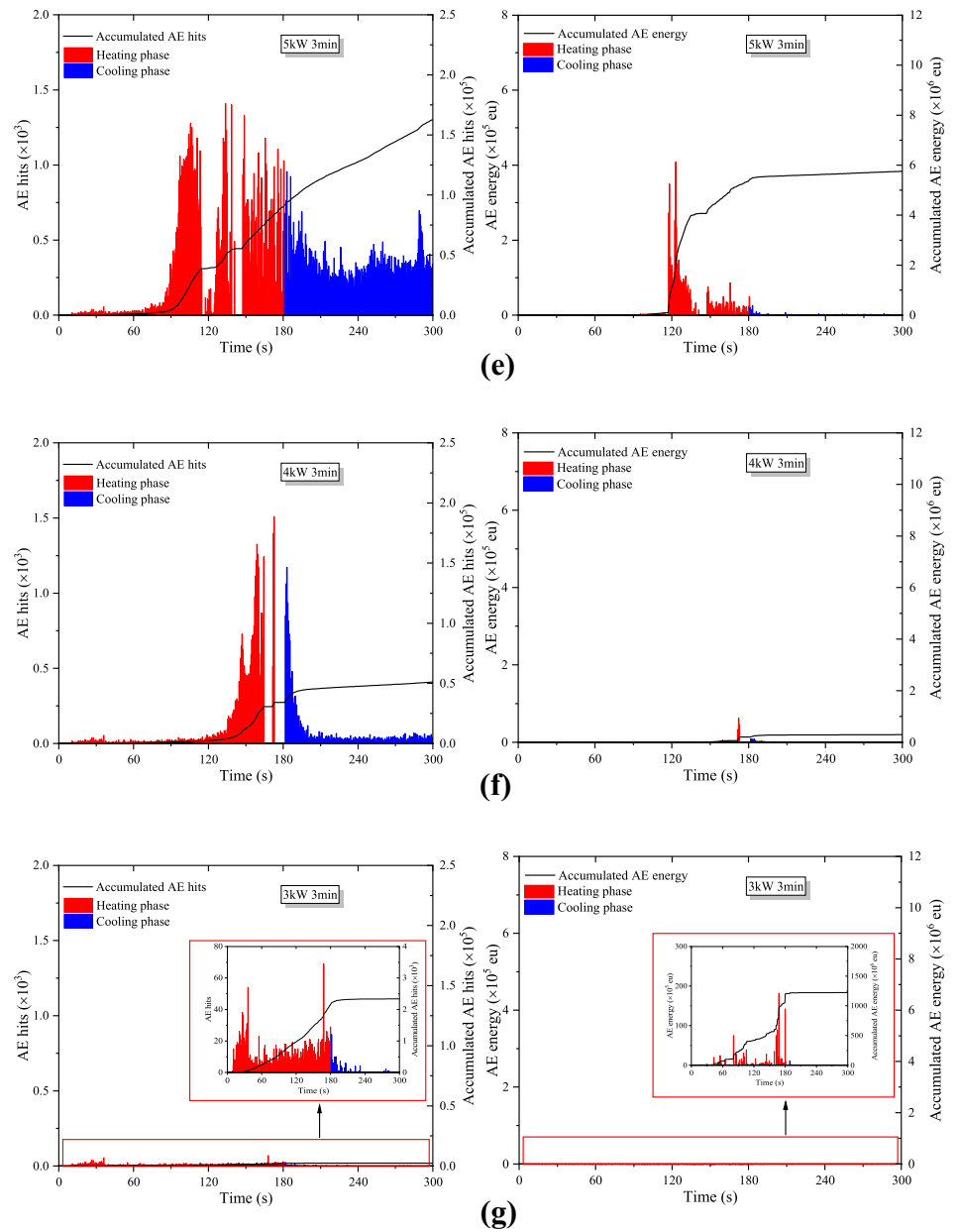
Fig. 6 (continued)

(e)

(f)

(g)

Table 2 AE count rate, hit rate, energy rate and event rate for microwave tests on granite

| Power (kW)	Time (min)	Max. temperature (°C)	Heating (min⁻¹)				Cooling (min⁻¹)			
			Counts	Energy	Hits	Events	Counts	Energy	Hits	Events
6	1	291	4406	522	1469	0	59	10	19	0
6	2	373	2,767,013	2,497,101	25,715	32	274,386	139,573	23,212	40
6	3	434	2,867,463	2,593,305	30,942	28	344,486	179,989	28,709	68
6	4	512	3,050,439	2,549,950	34,257	31	434,830	211,780	41,056	154
5	3	398	2,323,461	1,789,770	30,078	20	288,194	132,591	29,930	51
4	3	321	144,863	67,684	11,354	15	62,203	26,506	7066	16
3	3	267	2545	398	723	1	62	4	25	0
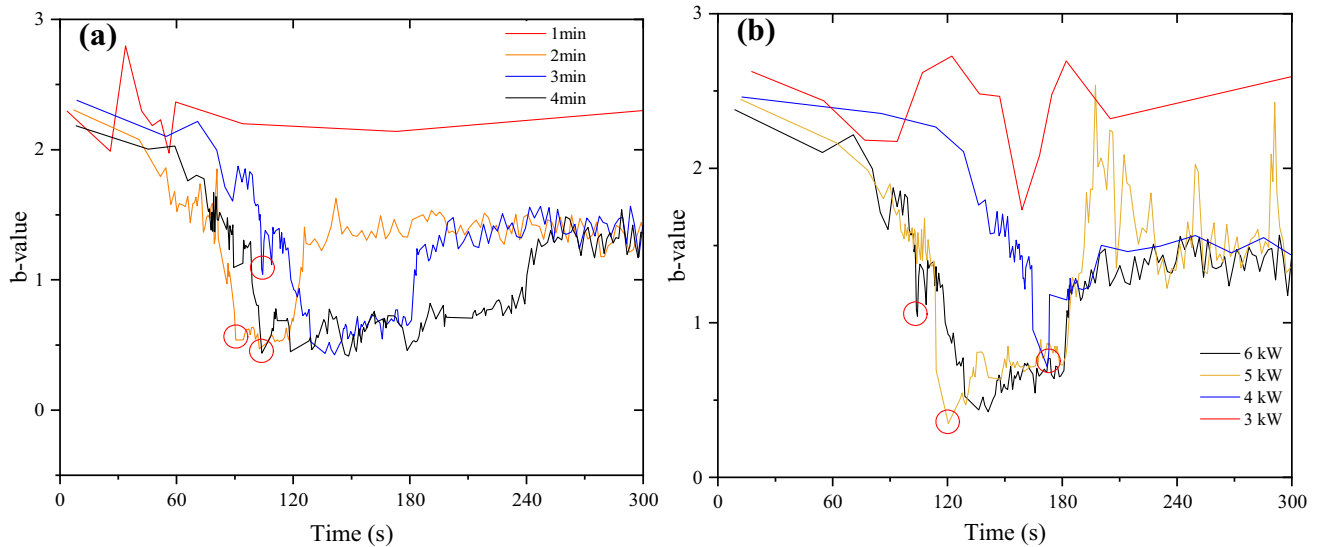
Fig. 7 Change of the b value in the microwave heating and cooling phases. **a** At 6 kW for 1–4 min, **b** at 3–6 kW for 3 min

microwave heating, the b value has a significant rebound and becomes almost unchanged in the cooling phase. The rebound value is even lower than the value of the rock at the beginning of heating. In this study, we define the steep drop in b value as the fluctuation of b value reaching 0.5 within 10 s. Figure 7b shows the relationship between the b value and time at 3–6 kW for 3 min. It is clear that the higher the microwave power, the earlier the b value started to drop dramatically, indicating an early fracturing time.

4.2 Failure Mode

The JCMS (Japan Construction Material Standards) crack classification method was adopted in this study to analyse the crack types, such as tensile cracks and shear cracks in the microwave heating and cooling phases (Zhai et al. 2020). It was conducted by employing two parameters of RA and AF. RA equals the rise time divided by the maximum amplitude, and AF equals AE ring-down count divided by the duration. In general, low AF and high RA values indicate the generation or development of shear cracks, and high AF and low RA values indicate the generation or development of tensile cracks (Zhang and Deng 2020).

Figure 8 shows the distribution of RA and AF of the specimen treated at 6 kW for 4 min. The results show that the microwave-induced rock failure during the heating and cooling phases is primarily tensile failure. The mechanism responsible for the thermal cracking is thus considered to be tensile fracturing.
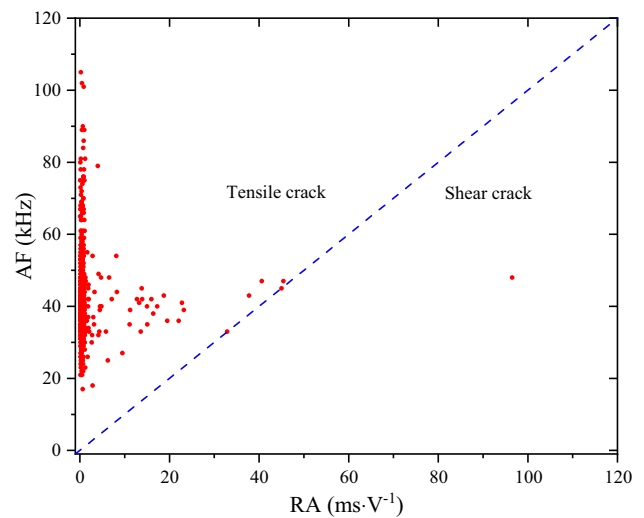

Fig. 8 Distribution of RA and AF of the granite specimen treated at 6 kW for 4 min

4.3 Contribution of Microwave Heating and Cooling Phases to Rock Damage

As discussed in Sect. 3.3 and shown in Table 2, a quantitative comparison of the AE energy rate, AE hits rate, AE counts rate and AE events rate generated during the microwave heating and the cooling phase highlights the differences between heating-induced and cooling-induced microcracking. The results show that for all the tests more accumulated AE energy rate was generated in the microwave heating phase than in the cooling phase. The AE energy rate in the microwave heating is more than 10 times that in the cooling phase. Therefore, it is concluded that the microwave

heating phase dominates the microwave-induced cracking. The observations of this study are contrary to the conventional heating and cooling tests, in which the fracturing can be cooling dominated (Browning et al. 2016). The reason might be that the conventional heating rate is low (up to 8 °C/min), which is much smaller than the microwave heating rate of 100–300 °C/min in this article. The specimens exposed to thermal shock are likely to crack violently. Another explanation is that in the cooling phase, the high

temperature zone in the centre of the specimens is under compression, inhibiting the generation of cracks.

4.4 Fracture Evolution

The location of a fracture source is determined using a non-linear iterative algorithm based on the arrival time difference received by different AE sensors. AE events can reflect the development and evolution of internal cracks in specimens
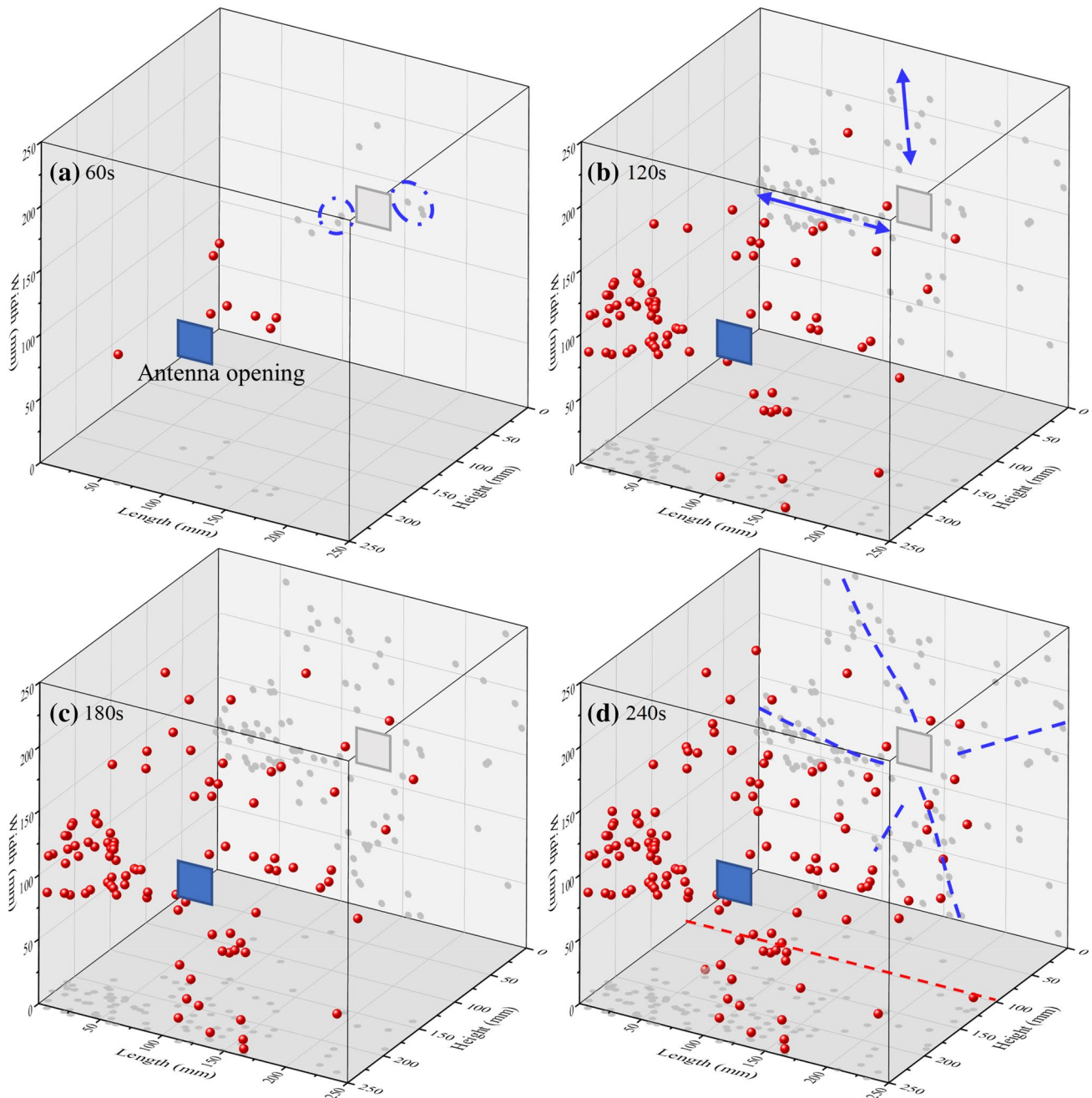

Fig. 9 Temporal–spatial distributions of AE sources of specimen treated at 6 kW for 4 min (the red ball represent the spatial events, and the grey ball represent the projection of the events on the back and underside)

treated by microwave. The temporal–spatial distributions of the AE sources for the specimen treated at 6 kW for 4 min are shown in Fig. 9. The red balls represent the spatial events and the grey balls represent the projection of the events on the back and underside. As shown in Fig. 9a, the AE events started from near the exterior of the open-ended microwave antenna, where the thermal gradient and stress were the greatest (Ma et al. 2021b). As the specimen was further heated, the AE events increased sharply when the heating time reached 120 s, due to the generation of a crack to the free surface. As shown in Fig. 9b, the AE events have two development trends, one is to develop towards the edge of the specimen, the other towards the centre of the antenna. When the rock specimen is further heated to 4 min, cracks simultaneously extended to the edge and the centre of the specimen. The maximum depth of the most AE events is about 15 cm when the specimen was treated for 4 min. This is in good agreement with the cutting test, which gives a maximum crack depth of 14.2 cm. As can be found in Fig. 9d, the spatial distribution of the AE sources is consistent with the crack pattern on the specimen.

It should be noted that some AE events located outside the specimen are not shown in Fig. 9. The AE positioning error can be explained as follow. (1) Some AE sources occurred at the same or close time. Therefore, it cannot be guaranteed that the signals arriving in each channel successively are the same point source signal (Gong et al. 2020). (2) In this study, the P-wave velocity was set to be a constant throughout the microwave heating and cooling phases. However, the velocity field is generally uneven and anisotropic. It will gradually decrease during the microwave heating, and the degree of P-wave reduction is different at different locations. Thus, the constant velocity assumption inevitably produced errors (Peng et al. 2018; Dong et al. 2017; Xue et al. 2021). (3) The AE signal will attenuate and distort in varying degrees in the phase of propagation, which makes it difficult to obtain the time difference.

5 Conclusions

In this study, the real-time fracturing of an alkali feldspar granite during the microwave heating and natural cooling phases was investigated using the AE technique. The AE characteristics, the evolution of fractures and the fracture modes in the heating and cooling phases were comprehensively studied. The main conclusions are drawn as follows:

(1) As either the microwave power level or the heating time increases, the alkali–feldspar granite were more fractured by the open-ended DLCWA at 6 kW. The high-power effect was validated by higher tempera-

ture, higher P-wave velocity reduction rate, higher AE energy and earlier fracturing.

(2) The accumulated AE energy and counts during the microwave heating phase are over 10 times higher than those in the cooling phase, suggesting that the microwave fracturing of the granite specimens is heating-dominated. The role of natural cooling in the fracturing process can be neglected.

(3) The microwave-induced rock fracturing is primarily tensile failure, due to the expansion of the high-temperature zone in the centre. Cracks initiated from the exterior of the antenna, where the thermal gradient and stress is the largest and propagated to the edge of the specimens. The use of AE measurement in localising fracture propagation is feasible.

Declarations

References

Aker E, Kühn D, Vavryčuk V, Soldal M, Oye V (2014) Experimental investigation of acoustic emissions and their moment tensors in rock during failure. Int J Rock Mech Min Sci 70:286–295. https://doi.org/10.1016/j.ijrmms.2014.05.003

Bai G, Sun Q, Jia H, Ge Z, Li P (2021) Variations in fracture toughness of SCB granite influenced by microwave heating. Eng Fract Mech. https://doi.org/10.1016/j.engfracmech.2021.108048

Browning J, Meredith P, Gudmundsson A (2016) Cooling-dominated cracking in thermally stressed volcanic rocks. Geophys Res Lett 43(16):8417–8425. https://doi.org/10.1002/2016gl070532

Chen J-H, Georgi D, Liu H-H, Jilin Z, Eppler G (2015) Assessing tensile strength of unconventional tight rocks using microwaving. In: Unconventional Resources Technology Conference, pp 1–13

Council NR (1994) Microwave processing of materials. Washington, DC, USA

Dong L, Sun D, Li X, Du K (2017) Theoretical and experimental studies of localization methodology for AE and microseismic sources without pre-measured wave velocity in mines. IEEE Access 5:16818–16828. https://doi.org/10.1109/access.2017.2743115

Du K, Li X, Tao M, Wang S (2020) Experimental study on acoustic emission (AE) characteristics and crack classification during rock fracture in several basic lab tests. Int J Rock Mech Min Sci. https://doi.org/10.1016/j.ijrmms.2020.104411

Feng X-T, Zhang J, Yang C, Tian J, Lin F, Li S, Su X (2021) A novel true triaxial test system for microwave-induced fracturing of hard

rocks. J Rock Mech Geotech Eng 13(5):961–971. https://doi.org/10.1016/j.jrmge.2021.03.008

Ge Z, Sun Q (2018) Acoustic emission (AE) characteristics of granite after heating and cooling cycles. Eng Fract Mech 200:418–429. https://doi.org/10.1016/j.engfracmech.2018.08.011

Ge Z, Sun Q (2021) Acoustic emission characteristics of gabbro after microwave heating. Int J Rock Mech Min Sci. https://doi.org/10.1016/j.ijrmms.2021.104616

Gong Q, Ding S, Wu F, Yin L (2020) Acoustic emission characteristics of ock fragmented by TBM cutter. J Beijing Univ Technol 46(1):42–50. https://doi.org/10.11936/bjutxb2018030016

Grosse CU, Ohtsu M (2008) Acoustic emission testing: basics for Research—Applications in Civil Engineering. Springer, Berlin. https://doi.org/10.1007/978-3-540-69972-9

Guo P, Wu S, Zhang G, Chu C (2021) Effects of thermally-induced cracks on acoustic emission characteristics of granite under tensile conditions. Int J Rock Mech Min Sci. https://doi.org/10.1016/j.ijrmms.2021.104820

Gutenberg B, Richter C (1950) Seismicity of the earth and associated phenomena. Geograph Rev 111(2):174–176

Hartlieb P, Grafe B, Shepel T, Malovyk A, Akbari B (2017) Experimental study on artificially induced crack patterns and their consequences on mechanical excavation processes. Int J Rock Mech Min Sci 100:160–169. https://doi.org/10.1016/j.ijrmms.2017.10.024

Hassani F, Nekoovaght PM, Gharib N (2016) The influence of microwave irradiation on rocks for microwave-assisted underground excavation. J Rock Mech Geotech Eng 8(1):1–15. https://doi.org/10.1016/j.jrmge.2015.10.004

Kahraman S, Canpolat AN, Fener M (2020) The influence of microwave treatment on the compressive and tensile strength of igneous rocks. Int J Rock Mech Min Sci 129:104303. https://doi.org/10.1016/j.ijrmms.2020.104303

Kahraman S, Sarbangholi FS, Balci C, Fener M, Karpuz C, Comakli R, Unver B, Ozcelik Y (2022) The effect of mineralogy on the microwave assisted cutting of igneous rocks. Bull Eng Geol Env 81(1):62. https://doi.org/10.1007/s10064-021-02561-3

Keshavarz M, Pellet FL, Loret B (2010) Damage and changes in mechanical properties of a gabbro thermally loaded up to 1,000°C. Pure Appl Geophys 167(12):1511–1523. https://doi.org/10.1007/s00024-010-0130-0

Kingman SW, Jackson K, Cumbane A, Bradshaw SM, Rowson NA, Greenwood R (2004) Recent developments in microwave-assisted comminution. Int J Miner Process 74(1–4):71–83. https://doi.org/10.1016/j.minpro.2003.09.006

Kong B, Wang E, Li Z, Wang X, Liu J, Li N (2016) Fracture mechanical behavior of sandstone subjected to high-temperature treatment and its acoustic emission characteristics under uniaxial compression conditions. Rock Mech Rock Eng 49(12):4911–4918. https://doi.org/10.1007/s00603-016-1011-3

Li N, Zhang S, Wang H, Wu S, Zou Y, Ma X, Zhou T (2021) Thermal shock effect on acoustic emission response during laboratory hydraulic fracturing in Laizhou granite. Rock Mech Rock Eng 54(9):4793–4807. https://doi.org/10.1007/s00603-021-02568-y

Li X, Wang S, Xia K, Tong T (2020a) Dynamic tensile response of a microwave damaged granitic rock. Exp Mech. https://doi.org/10.1007/s11340-020-00677-3

Li X, Wang S, Xu Y, Yao W, Xia K, Lu G (2020b) Effect of microwave irradiation on dynamic mode-I fracture parameters of Barre granite. Eng Fract Mech. https://doi.org/10.1016/j.engfracmech.2019.106748

Lu G-M, Feng X-T, Li Y-H, Zhang X (2019) The microwave-induced fracturing of hard rock (journal article). Rock Mech Rock Eng. https://doi.org/10.1007/s00603-019-01790-z

Lu G, Sun Z, Zhou J, Chen K, Li F (2021) Effect of microwave irradiation on computed tomography and acoustic emission

characteristics of hard rock. Geotech Geol Eng 39(1):411–424. https://doi.org/10.1007/s10706-020-01500-5

Lyu C, Liu J, Wu Z, Liu H, Xiao F, Zeng Y (2021) Experimental study on mechanical properties, permeability and acoustic emission characteristics of gypsum rock under THM coupling. Rock Mech Rock Eng 54(11):5761–5779. https://doi.org/10.1007/s00603-021-02586-w

Ma X, Westman E, Slaker B, Thibodeau D, Counter D (2018) The b-value evolution of mining-induced seismicity and mainshock occurrences at hard-rock mines. Int J Rock Mech Min Sci 104:64–70. https://doi.org/10.1016/j.ijrmms.2018.02.003

Ma Z, Zheng Y, Zhao X, Li J, Zhao J (2021a) A dielectric-loaded converging waveguide antenna for microwave fracturing of hard rocks. IEEE Trans Antennas Propag. https://doi.org/10.1109/TAP.2021.3138425 (**In Press**)

Ma ZJ, Zheng YL, Li XZ, Zhao XB, He L, Zhao QH, He JL, Li JC (2021b) Design and performance of an open-ended converging microwave antenna in fracturing biotite diorite at low microwave power levels. Geomech Geophys Geo-Energy Geo-Resour. https://doi.org/10.1007/s40948-021-00291-0

Nava FA, Márquez-Ramírez VH, Zúñiga FR, Ávila-Barrientos L, Quinteros CB (2016) Gutenberg-Richter b-value maximum likelihood estimation and sample size. J Seismolog 21(1):127–135. https://doi.org/10.1007/s10950-016-9589-1

Peng J, Rong G, Yao M, Wong LNY, Tang Z (2018) Acoustic emission characteristics of a fine-grained marble with different thermal damages and specimen sizes. Bull Eng Geol Env 78(6):4479–4491. https://doi.org/10.1007/s10064-018-1375-6

Ren Y, Vavryčuk V, Wu S, Gao Y (2021) Accurate moment tensor inversion of acoustic emissions and its application to Brazilian splitting test. Int J Rock Mech Min Sci. https://doi.org/10.1016/j.ijrmms.2021.104707

Wang S, Xu Y, Xia K, Tong T (2020) Dynamic fragmentation of microwave irradiated rock. J Rock Mech Geotech Eng. https://doi.org/10.1016/j.jrmge.2020.09.003

Wei W, Shao Z, Zhang Y, Qiao R, Gao J (2019) Fundamentals and applications of microwave energy in rock and concrete processing – a review. Appl Therm Eng 157:113751. https://doi.org/10.1016/j.applthermaleng.2019.113751

Whittles DN, Kingman SW, Reddish DJ (2003) Application of numerical modelling for prediction of the influence of power density on microwave-assisted breakage. Int J Miner Process 68(1–4):71–91. https://doi.org/10.1016/s0301-7516(02)00049-2

Wu Y, Li X-Z, Huang Z, Xue S (2021) Effect of temperature on physical, mechanical and acoustic emission properties of Beishan granite, Gansu Province, China. Nat Hazards 107(2):1577–1592. https://doi.org/10.1007/s11069-021-04647-3

Xu T, Yuan Y, Heap MJ, Zhou G-L, Perera MSA, Ranjith PG (2021) Microwave-assisted damage and fracturing of hard rocks and its implications for effective mineral resources recovery. Miner Eng 160:106663. https://doi.org/10.1016/j.mineng.2020.106663

Xue C, Xu G, Wang X, Gao J, Gao D (2021) Error analysis and correction of multi-sensor cluster methods for acoustic emission source localization. Ultrasonics 115:106438. https://doi.org/10.1016/j.ultras.2021.106438

Yang B-g, Gao M-z, Xie J, Liu J-j, Wang F, Wang M-y, Wang X, Wen X-y, Yang Z-y (2022) Exploration of weakening mechanism of uniaxial compressive strength of deep sandstone under microwave irradiation. J Central South Univ 29(2):611–623. https://doi.org/10.1007/s11771-022-4910-3

Yang S-Q, Tian W-L, Elsworth D, Wang J-G, Fan L-F (2020) An experimental study of effect of high temperature on the permeability evolution and failure response of granite under triaxial compression. Rock Mech Rock Eng 53(10):4403–4427. https://doi.org/10.1007/s00603-019-01982-7

Yin LJ, Gong QM, Ma HS, Zhao J, Zhao XB (2014) Use of indentation tests to study the influence of confining stress on rock fragmentation by a TBM cutter. Int J Rock Mech Min Sci 72:261–276. https://doi.org/10.1016/j.ijrmms.2014.07.022

Zhai S, Su G, Yin S, Yan S, Wang Z, Yan L (2020) Fracture evolution during rockburst under true-triaxial loading using acoustic emission monitoring. Bull Eng Geol Env 79(9):4957–4974. https://doi.org/10.1007/s10064-020-01858-z

Zhang Y, Zhao G-F, Li Q (2020) Acoustic emission uncovers thermal damage evolution of rock. Int J Rock Mech Min Sci. https://doi.org/10.1016/j.ijrmms.2020.104388

Zhang Z-H, Deng J-H (2020) A new method for determining the crack classification criterion in acoustic emission parameter analysis. Int J Rock Mech Min Sci. https://doi.org/10.1016/j.ijrmms.2020.104323

Zhao QH, Zhao XB, Zheng YL, Li JC, He L, Zou CJ (2020) Microwave fracturing of water-bearing sandstones: heating characteristics and bursting. Int J Rock Mech Min Sci. https://doi.org/10.1016/j.ijrmms.2020.104495

Zheng Y-l, He L (2021) TBM tunneling in extremely hard and abrasive rocks: Problems, solutions and assisting methods. J Central South Univ 28(2):454–480. https://doi.org/10.1007/s11771-021-4615-z

Zheng YL, Ma Z, Zhao X, He L (2020) Experimental investigation on the thermal, mechanical and cracking behaviours of three igneous rocks under microwave treatment. Rock Mech Rock Eng 53(8):3657–3671. https://doi.org/10.1007/s00603-020-02135-x

Zheng YL, Ma ZJ, Yang SQ, Zhao XB, He L, Li JC (2021) A microwave fracturability index (MFI) of hard igneous rocks. Int J Rock Mech Min Sci. https://doi.org/10.1016/j.ijrmms.2020.104566

Zheng YL, Zhang QB, Zhao J (2017) Effect of microwave treatment on thermal and ultrasonic properties of gabbro. Appl Therm Eng 127:359–369. https://doi.org/10.1016/j.applthermaleng.2017.08.060